

# Population inversion of a NAHS mixture adsorbed into a cylindrical pore

Felipe Jiménez-Ángeles, Yurko Duda, Gerardo Odriozola, and Marcelo Lozada-Cassou

*Programa de Ingeniería Molecular, Instituto Mexicano del Petróleo,*

*Lázaro Cárdenas 152, 07730 México, D. F., México*

(Dated: October 24, 2018)

A cylindrical nanopore immersed in a non-additive hard sphere binary fluid is studied by means of integral equation theories and Monte Carlo simulations. It is found that at low and intermediate values of the bulk total number density the more concentrated bulk species is preferentially absorbed by the pore, as expected. However, further increments of the bulk number density lead to an abrupt population inversion in the confined fluid and an entropy driven prewetting transition at the outside wall of the pore. These phenomena are a function of the pore size, the non-additivity parameter, the bulk number density, and particles relative number fraction. We discuss our results in relation to the phase separation in the bulk.

PACS numbers: 61.30.Hn,61.46.Fg

## I. INTRODUCTION

Fluids in confinement appear in many disciplines ranging from biophysics to material science. Nanotubes, molecular channels formed by transmembrane proteins, micelles, micropores and nanopores in rocks are some examples of confining structures of nanometric dimensions. Hence, understanding the effect of confinement on fluids physicochemical properties is relevant for a broad variety of technological areas such as catalysis, oil recovery, and drugs delivery<sup>1</sup>, to cite a few. Some examples of phenomena associated with confinement are capillary condensation<sup>2</sup>, new phases of water<sup>3</sup> and wetting-drying transition<sup>4</sup>. In charged complex fluids, confinement may produce the formation of a 2-D array stack of polyelectrolytes<sup>5,6</sup> and closed spherical and cylindrical charged nanopores induce charge separation of a confined electrolyte<sup>7,8</sup>.

Capillary condensation and wetting are, perhaps, the most studied phase transitions of confined fluids<sup>9,10</sup>. When a vapor is confined, e.g. by a nanopore, in the appropriate conditions, it condenses, such that this liquid is in equilibrium with the bulk vapor: This phenomenon is known as capillary condensation. On the other hand, the fluid at a fluid-wall interface may present two different regimes of adsorption: By increasing the fluid number density, i.e., as the fluid approaches to its saturation density,  $\rho_{\text{sat}}$ , the adsorbed fluid forms droplets (non-wetting) or spreads (wetting) on the surface, producing a film of finite thickness of a condensed phase, i.e., 1) In the non-wetting regime the adsorbed fluid forms a thin layer, which increases slightly as the fluid approaches to  $\rho_{\text{sat}}$ . At  $\rho_{\text{sat}}$  the fluid condenses, producing a macroscopic droplet, thus giving rise to a sudden increase of adsorption. 2) At the prewetting regime, a thick layer of fluid coexists with a thin one, competing to cover the wall as the fluid density goes to  $\rho_{\text{sat}}$ . At  $\rho_{\text{sat}}$  a thick layer of fluid covers the wall, i.e., wetting.

Capillary condensation and wetting have been widely studied in pure simple fluids with fluid-fluid and confining wall-fluid attractive interactions<sup>9,10,11,12,13,14,15</sup>. On

the other hand, entropy driven wetting and capillary transitions of hard-core interacting fluids have been addressed just recently<sup>16</sup>. Capillary phenomena for confined complex fluids have been also addressed through the Asakura-Oosawa (AO) model<sup>17,18,19</sup>. In this model it is considered a mixture of hard-sphere colloids and point particles and has been used to study capillary condensation<sup>17,18</sup> and evaporation<sup>20,21</sup>.

Non additive hard sphere (NAHS) fluids have been studied in the past for different confinement conditions<sup>22,23,24</sup>. It is well known that this model fluid exhibits a two phase separation in bulk<sup>25</sup>, hence, capillary and surface phase transitions, inside and outside of a nanopore, are expected upon approaching to the bulk coexistence curve. Here we will focus on the confinement induced phase transitions of a NAHS binary mixture inside and outside a cylindrical nanopore (athermal and exclusively driven by entropy). We compare these two confinement induced phase transition diagrams with that for a bulk fluid. It should be pointed out that the NAHS model separates into two *dense* phases: one phase rich in species A and poor in species B, while the other is oppositely composed, i.e., rich in species B and poor in species A. On the other hand, in confinement capillary condensation and evaporation occur simultaneously. Thus, we will refer to the capillary induced phase transition reported here as population inversion since the phases are equally dense and oppositely composed.

## II. MODEL AND THEORY

The interest in NAHS is motivated by the observed nonadditivity in real mixtures<sup>26</sup> and by the belief that large nonadditivity plays an essential role in the structure of some liquid alloys<sup>27</sup>. The limiting case of the NAHS model (so-called, Widom Rowlinson penetrable hard sphere mixture) can be used to describe condensation phenomena<sup>28,29</sup>. NAHS pair potential has been successfully applied to the study of the morphology of composite polymer particles<sup>30</sup>, the solubility of molecu-

lar additives in different solvents<sup>31</sup>, the microstructure of micelles<sup>32</sup>, and for the description of gas-gas phase transition at high pressure observed in mixtures of rare gases<sup>33</sup>. Here we use the NAHS as a simple way of modelling affinity between particles of the same species and phobicity for particles of a different one<sup>22,23,24,34,35,36,37</sup>, such as, for example, a colloidal phase of oil interacting with a water soluble polymer. The model distinguishes between two species (A and B) by defining a closest approach distance between two particles of species  $i$  and  $j$ ,  $\sigma_{ij}$ , as follows:

$$\begin{aligned}\sigma_{AA} &= \sigma_{BB} = \sigma \\ \sigma_{AB} &= \sigma(1 + \Delta)\end{aligned}\quad (1)$$

being  $\sigma$  the diameter of the particle, taken as the unit length, and  $\Delta$  the non additivity parameter. In bulk, for  $\Delta > 0$  the mixture may separate in two phases, each of which consists predominantly of one species, A or B. For the sake of simplicity we consider here the symmetrical case of the NAHS model, although the main conclusions of our work qualitatively do not depend on the size asymmetry. The main features of the NAHS model are depicted in Fig. 1. Note that this model is *athermal* since we are dealing with hard sphere interactions.

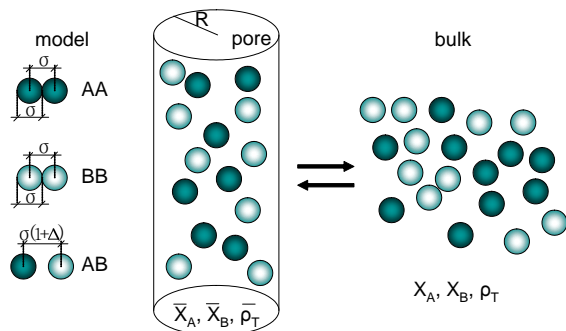


FIG. 1: Set up of the NAHS model and the system under study. Dark and light gray spheres represent species A and B, respectively.

Let us consider the absorption of a binary mixture of NAHS particles by a cylindrical pore of radius  $R$  and infinite length, immersed in a symmetrical NAHS bulk fluid. Hence, the confined fluid and the infinite reservoir are at the same chemical potential. The two species A and B, are at a number density  $\rho_i$  ( $i = A, B$ ), with the fluid total number density  $\rho_T = \rho_A + \rho_B$ , and particles relative fraction  $X_i = \frac{\rho_i}{\rho_T}$ . The relative fraction for species  $i$  inside the pore is defined as  $\bar{X}_i = \frac{\bar{\rho}_i}{\bar{\rho}_T}$ , being  $\bar{\rho}_T = \bar{\rho}_A + \bar{\rho}_B$ , where  $\bar{\rho}_i$  is the average number density of species  $i$  inside the pore (see Fig. 1). Note that because of the model symmetry, only the interval  $0 \leq X_A \leq 0.5$  needs to be considered. In this work, this system is studied by two methods: Integral equation theory and Monte Carlo (MC) simulations.

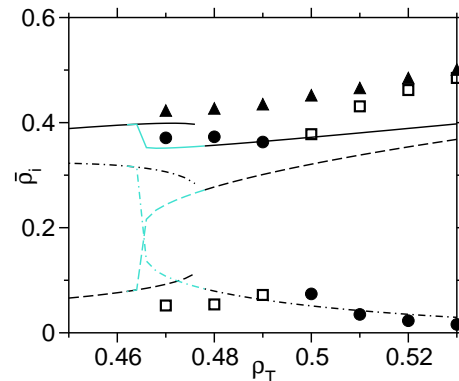


FIG. 2: Absorption curves ( $\bar{\rho}_i$ , with  $i = A, B, T$ ) as a function of  $\rho_T$ , for  $R = 3.5$ ,  $\Delta = 0.2$  and  $X_A = 0.06$ :  $\square$ ,  $\bullet$  and  $\blacktriangle$  symbols are, respectively, MC results for  $\bar{\rho}_A$ ,  $\bar{\rho}_B$  and  $\bar{\rho}_T$ , whereas the dashed, dot-dashed and solid lines are the corresponding results from HNC/PY theory. Black lines are obtained by increasing  $\rho_T$ , whereas the light branches show a hysteresis interval obtained upon decreasing  $\rho_T$  from values above the upper transition.

Liquid theories based on the Ornstein-Zernike integral equation have been applied to both, charged and uncharged fluids confined by planar, cylindrical and spherical nanopores, showing, in general, good agreement with computer simulations<sup>7,23,24,38</sup>. The method we use to derive integral equations for confined fluids is based on the equivalence between particles and fields<sup>39</sup>. Thus, the Ornstein-Zernike equation for inhomogeneous fluids is obtained by considering the cylindrical pore as one more fluid species ( $\alpha$ ) at infinite dilution ( $\rho_\alpha \rightarrow 0$ ). From this inhomogeneous fluid integral equation, the hypernetted chain/Percus-Yevick (HNC/PY) can be readily derived for a two species NAHS fluid confined by a cylindrical pore, which relates the reduced concentration profile of species  $i$  inside the cylinder,  $g_{\alpha i}(r)$ , the total correlation function,  $h_{\alpha i}(r) \equiv g_{\alpha i}(r) - 1$ ; and the direct correlation function,  $c_{mi}(s)$ , i.e.,

$$g_{\alpha i}(r) = \exp \left\{ -\beta u_{\alpha i}(r) + \sum_{m=1}^2 \rho_m \int h_{\alpha m}(r') c_{mi}(s) dr' \right\} \quad (2)$$

where  $r$  and  $r'$  are two radial cylindrical coordinates with its origin at the center of the pore,  $s = |\mathbf{r} - \mathbf{r}'|$  is the relative distance between two particles of species  $i$  and  $m$  at  $\mathbf{r}$  and  $\mathbf{r}'$ , respectively, and  $dr'$  is the volume element;  $\rho_m$  is the bulk number density of species  $m$ ;  $\beta = 1/(k_B T)$ , where  $k_B$  is the Boltzmann constant and  $T$  is the absolute temperature;  $u_{\alpha i}(r)$  is the direct interaction potential between a particle of species  $i$  and the pore, which is simply a hard-core interaction potential being  $u_{\alpha i}(r) = \infty$  for  $r \geq R - \sigma/2$ ;  $c_{mi}(s)$  is approximated by the Percus-Yevick (PY) closure<sup>40</sup>. The mean number density of species  $i$  inside the pore,  $\bar{\rho}_i$ , is computed as

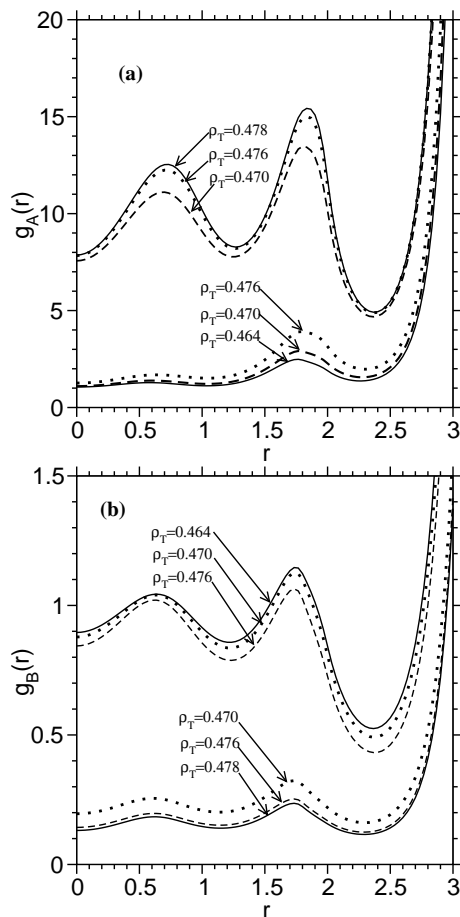


FIG. 3: Theoretical reduced concentration profiles inside the cylindrical nanopore,  $g_A(r)$  and  $g_B(r)$ , for species A and B, respectively; and for  $R = 3.5$ ,  $\Delta = 0.2$ ,  $X_A = 0.06$ , and  $\rho_T = 0.64, 0.70, 0.76, 0.78$ . The concentration profiles for  $\rho_T = 0.70$  and  $0.76$  correspond with the two branches of  $\bar{\rho}_i$  vs  $\rho_T$ , in Fig. 2, according to the color line.

$$\bar{\rho}_i = \frac{\bar{N}_i}{V_p} = \frac{2\rho_i}{R^2} \int_0^{R-\sigma/2} g_{\alpha i}(r) r dr \quad (3)$$

being  $\bar{N}_i = 2\pi L \rho_i \int_0^{R-\sigma/2} g_{\alpha i}(r) r dr$  the number of particles of species  $i$  absorbed into the pore,  $V_p = \pi L R^2$  the pore's volume, and  $L$  the pore's length. For the bulk fluid the HNC/PY equation is derived simply by considering the  $\alpha$  species particle to be equal to one of the fluid species, say,  $\alpha = A$  or  $\alpha = B$ . For the bulk fluid, it is interesting to note that there is a region of the  $(X_A, \rho_T)$  space where HNC/PY bifurcates into two solutions and in a hysteretical cycle, such that the cycle region is within the coexistence and spinodal curves.

MC simulations are performed in the modified Gibbs ensemble<sup>41</sup>. We considered the NAHS mixture in the bulk cubic simulation cell and absorbed inside the cylindrical pore, see Fig. 1. Thus the absorbed and bulk fluids are in equilibrium. Unlike the usual Gibbs ensemble

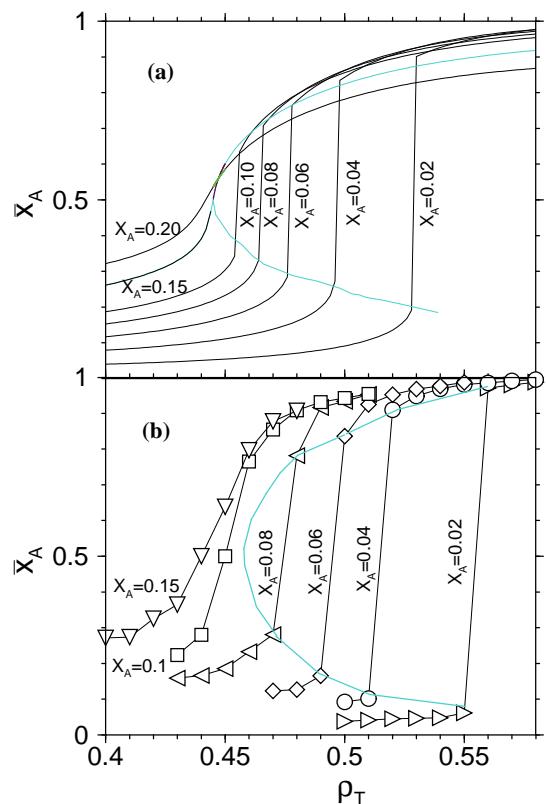


FIG. 4: Relative A fraction,  $\bar{X}_A$ , as a function of  $\rho_T$ , for  $R = 3.5$ ,  $\Delta = 0.2$  and for the indicated bulk relative fraction,  $X_A$ : (a) from HNC/PY theory and (b) from MC simulations.

simulation, the relative fraction ( $X_A$ ) and bulk number density ( $\rho_T$ ) of the NAHS fluid are fixed, hence, we only perform creation and annihilation of particles in the nanopore according with bulk conditions. The length of the bulk box side and the cylinder axis are large enough to avoid size effects. The number density and relative fraction of the absorbed fluid have been calculated and analyzed by the histogram method. Standard semi-grand canonical MC simulations<sup>42</sup> are performed for obtaining the two-phase separation diagram of the bulk fluid. Our MC results for the bulk are in agreement with those reported by Amar<sup>25</sup>.

### III. RESULTS

#### A. Inside the cylindrical pore: Population Inversion

A cylindrical pore with  $R=3.5$  and a NAHS fluid with  $\Delta = 0.2$  are considered. It should be pointed out, however, that all the phenomena discussed here are observed whenever  $\Delta > 0$ . Fig. 2 shows the absorbed fluid number densities  $\bar{\rho}_A$ ,  $\bar{\rho}_B$ , and  $\bar{\rho}_T$ , as a function of the bulk total density,  $\rho_T$ , for a given relative A-particle fraction,  $X_A$ . For low values of  $\rho_T$  species B is preferably absorbed

by the pore ( $\bar{\rho}_B \gg \bar{\rho}_A$ ), as expected since  $X_B = 0.94$ . Interestingly,  $\rho_A$  is lower than  $\bar{\rho}_A$  for all  $\rho_T$ , which is atypical for purely repulsive interactions<sup>38</sup>. For a certain transition bulk number density,  $\rho_T^t$ ,  $\bar{\rho}_B$  has a discontinuous drop, while  $\bar{\rho}_A$  has the opposite behavior. Related phenomena have been observed with the confined AO model<sup>17,18,20,21</sup>. In that case, the transition can be explained by an effective colloid-colloid attractive interaction originated by the presence of polymers. Our case can be seen as a simultaneous A-species condensation and B-species evaporation. Furthermore, no preferential attraction is present because of the model symmetry. We refer to this phenomenon as *population inversion* (PI), i.e., for  $\rho_T < \rho_T^t$ ,  $\bar{\rho}_B \gg \bar{\rho}_A$  and for  $\rho_T > \rho_T^t$ ,  $\bar{\rho}_A \gg \bar{\rho}_B$ , and, we believe, this phenomenon is related to i) the catastrophic inversion of adsorbed water-oil emulsions<sup>43</sup> and ii) the selective adsorption of two nearly similar liquids by a membrane<sup>44</sup>.

The HNC/PY and MC results agree in this prediction. However the MC results for  $\bar{\rho}_T$  are systematically higher than those from HNC/PY, due to the unavoidable approximations in many-body theories. More interesting is that  $\rho_T^t$  from HNC/PY is lower than that from MC. This is because HNC/PY absorption of A-particles is higher than that of MC and, hence, there are more A-B pairs inside the pore, which in turn gives rise to a higher excluded volume and this prompts the transition: In the NAHS model AB pairs have higher excluded volume than AA or BB pairs. Notice that the MC transition occurs when its  $\bar{\rho}_A$  reaches around the same value as that of HNC/PY at the transition.

Black lines in Fig. 2 are successive solutions of Eq. (2) obtained by increasing  $\rho_T$ . On the other hand, the light branches correspond to the solutions calculated by decreasing  $\rho_T$  from above the  $\rho_T^t$  value. Notice, that both solutions coincide in almost all the studied interval of  $\rho_T$ , however there is an interval within which Eq. (2) has two solutions, i.e., an hysteresis cycle is found. These two solutions imply the presence of metastable states and two coexisting phases inside the cylindrical nanopore. MC results qualitatively confirm the presence of hysteresis, although the  $\rho_T$  interval is narrower ( $\Delta\rho_T \approx 0.01$ ).

Fig. 3 shows the reduced concentration profiles obtained from HNC/PY,  $g_{\alpha i}(r)$ , for both species ( $i = A, B$ ), inside the cylindrical nanopore. The solid lines are concentration profiles around the PI transition. In Fig. 3a, near  $\rho_T = 0.464$ , as we increase  $\rho_T$  we see a sudden increase in the species A population, inside the pore, when going from  $\rho_T = 0.476$  to  $\rho_T = 0.478$ . Because of the hysteretical nature of the PI transition, when decreasing the bulk concentration there is a sudden decrease of A species concentration below  $\rho_T = 0.470$ . In Fig 3 the corresponding hysteretical behavior of the B species is seen. Of course, an increase in species A implies a decrease in species B, and viceversa. This concentration interval correspond to hysteresis cycle shown in Fig.2: The light branches correspond to the decreasing concentration profiles in Fig. 3. Thus, for  $\rho_T \lesssim 0.464$  and  $\rho_T \gtrsim 0.476$  a sin-

gle solution is found, whereas, within this interval ( $0.464 \lesssim \rho_T \lesssim 0.476$ ) two families of solutions are found. Notice that only slight changes of  $g_A(r)$  and  $g_B(r)$  occur before and after the jump, either by increasing or decreasing  $\rho_T$ . The transition is seen by an increase (decrease) of  $g_A(r)$  ( $g_B(r)$ ) of about an order of magnitude. Both species, on the other hand, show a three-layer structure inside the nanopore.

Fig. 4 shows results from HNC/PY integral equations theory and MC simulations for the relative fraction of species A inside the cylinder,  $\bar{X}_A$ , as a function of the bulk total number density,  $\rho_T$ , for a set of values of the A species bulk relative fraction,  $X_A$ , such that  $X_A < X_B$ . The light curve defines the transition points. Notice that this curve is not a coexistence curve, but defines an instability region. The PI is observed only for  $X_A$  below a critical value,  $X_A^c$ . The critical isopleth predicted by MC simulations is  $X_A^c \approx 0.14$  with a consolute point at  $\rho_T^c \approx 0.451$ , whereas integral equations predict  $X_A^c \approx 0.13$  and  $\rho_T^c \approx 0.46$ . Our analysis of model parameters indicates that  $X_A^c$  depends on  $R$  and  $\Delta$  in a nontrivial way.

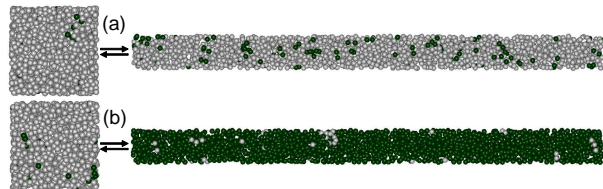


FIG. 5: Snapshots of typical MC configurations for the confined fluid. (a)  $\rho_T = 0.55 \lesssim \rho_T^t$  and (b)  $\rho_T = 0.56 \gtrsim \rho_T^t$ . Dark and light gray spheres represent species A and B, respectively. The left square boxes are the bulk snapshots which are in equilibrium with their respective confined fluids, in the cylindrical boxes. In both cases  $X_A = 0.02$ ,  $R = 3.5$ , and  $\Delta = 0.2$ .

Fig. 5 shows two snapshots, before and after the population inversion transition, for  $X_A = 0.02$ . Note that, although the bulk number densities are very close in both cases, the fluid inside the cylindrical pore dramatically changes its composition: In (a)  $\bar{\rho}_A = 0.03$  and  $\bar{\rho}_B = 0.461$ , whereas in (b)  $\bar{\rho}_A = 0.496$  and  $\bar{\rho}_B = 0.015$ .

The bulk NAHS fluid exhibits a fluid-fluid two phase separation (TPS)<sup>25</sup>. In Fig. 6 we show MC (black circles) and HNC/PY (solid light line) transition number densities,  $\rho_T^t$ , for the bulk fluid, as a function of  $X_A$ . Above the bulk TPS coexistence curve the fluid may separate into a rich A-species phase and a rich B-species phase. Below the curve the fluid is homogeneous. Between the coexistence (light) TPS and spinodal curves (dotted) a metastable homogeneous fluid is found. Also in Fig. 6 we show the MC and HNC/PY transition number densities,  $\rho_T^t$  as a function of  $X_A$ , at which there is a PI inside the cylindrical pore, i.e.,  $\bar{X}_A > \bar{X}_B$ , by increasing  $\rho_T$ , or  $\bar{X}_A < \bar{X}_B$ , by decreasing  $\rho_T$ . From the HNC/PY approach, the black solid and dashed lines are constructed with the transition points at which PI occurs by increas-

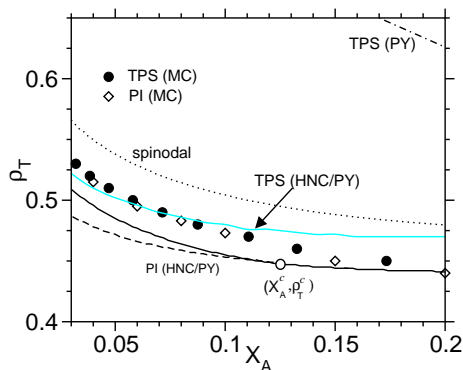


FIG. 6: Transition number density for the bulk two-phase separation (TPS) and for the population inversion (PI) of a NAHS fluid ( $\Delta = 0.2$ ) inside the cylindrical nanopore ( $R = 3.5$ ). The black circles and light curve are the MC and HNC/PY results for the bulk TPS, respectively. White diamonds and the black solid line are the MC and HNC/PY PI diagrams, respectively. The black solid and dashed lines defines the upper and bottom number density transitions, i.e., the limits of hysteresis. The theoretical consolute point,  $X_A^c \approx 0.13$ , is defined by the point where the black solid and dashed line converge. The dotted line is the HNC/PY bulk spinodal, whereas the black dotted-dashed line is the bulk TPS from PY integral equations theory. The PI consolute point  $(X_A^c, \rho_T^c)$  is signaled by an open circle.

ing/decreasing  $\rho_T$ , i.e., the hysteresis cycle pointed out in Figs. 2 and 3 is defined by the region between the solid and dashed lines. These two lines converge at the consolute point, i.e.,  $X_A^c \approx 0.13$ . For  $X_A > X_A^c$ , there is still a PI but it happens in a continuous way as  $\rho_T$  increases, i.e., there is not a sudden transition. According to the HNC/PY approach, the PI curve is shifted towards lower  $\rho_T$  values respect to the TPS curve, i.e., as  $\rho_T$  increases first occurs a PI inside the pore and later a TPS in the bulk. A closer inspection of MC data clearly confirm this prediction. The black dot-dashed at the right upper corner is the PY transition curve for the bulk TPS, and is included for reference.

Although not shown, for a fixed value of  $R$ , PI curves shift towards lower bulk number densities as  $\Delta$  increases, while the consolute point is at lower  $X_A$  values, responding to the higher volume demand of the A-B coordinates. At constant  $\Delta$ , the PI transition diagram is displaced to higher  $\rho_T$  values as  $R$  increases, whereas the consolute point shifts towards higher  $X_A$  values, because there is more accessible volume inside the pore.

### B. Outside the cylindrical pore: Wetting-like transition

The NAHS fluid in contact with the outside surface of the cylindrical nanopore was also studied by means of integral equations. Fig. 7 shows the reduced concentration profiles for both species, at the outside surface of the

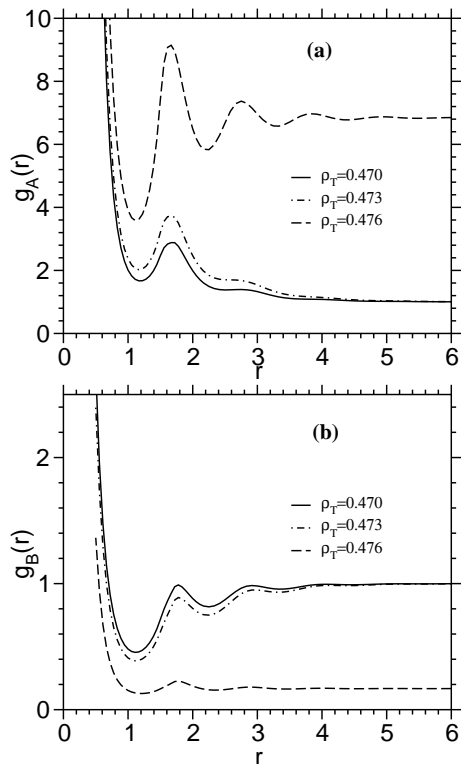


FIG. 7: Theoretical reduced concentration profiles outside the cylindrical nanopore,  $g_A(r)$  and  $g_B(r)$ , for species A and B, respectively; and for  $R \rightarrow \infty$ ,  $\Delta = 0.2$ ,  $X_A = 0.10$ , and  $\rho_T = 0.470, 0.473, 0.476$ .

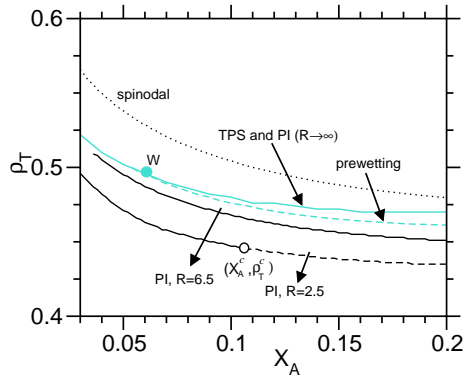


FIG. 8: Theoretical EDPW transition curve for  $R = \infty$  (dashed light) and PI curves for  $R = 2.5, 6.5$  (solid black), and  $\infty$  (solid light). Also is plotted the bulk spinodal curve (black dotted), while the TPS coexistence curve coincides with the PI for  $R \rightarrow \infty$  (solid light). The PI consolute point  $(X_A^c, \rho_T^c)$  is signaled by an open circle. The filled light circle is the converging point of the prewetting and TPS curves. In all cases  $\Delta = 0.2$ .

cylindrical nanopore, for  $\rho_T = 0.470$  and  $0.473$  (below the bulk TPS coexistence curve) and for  $\rho_T = 0.476$  (slightly above the bulk TPS coexistence curve). For this inhomogeneous fluid, below the TPS, we found a preferable adsorption of the less concentrated A-particles, which like

to be next to the cylinder. This can be seen by the high and increasing value of  $g_A(r)$  on the cylinder's surface, and the sudden long range correlation of particles A with respect to the cylinder surface, whereas  $g_B(r)$  decreases, as  $\rho_T$  increases. In order to evaluate this phenomenon we define the adsorption at the cylinder outside surface as

$$\Gamma_i = 2\pi \int_{R+a/2}^{\infty} \rho_i [g_i(r) - 1] r dr \quad (4)$$

with  $i = A, B$ , the species label.

Above a certain value of  $X_A = X_A^w$ , we find a bulk total number density,  $\rho_T^{pw}$  (below the PI and TPS transition curves), for which the adsorption on the outside cylinder's surface of A-particles is higher than for B-particles, i.e.,  $\Gamma_A > \Gamma_B$ . In Fig. 8, we constructed the prewetting line with this criterion. This phenomenon is similar to the prewetting occurring nearby the liquid-gas coexistence which, by increasing  $\rho_T$ , becomes wetting. Since there is not a surface-fluid attractive energetic contribution, we refer to this phenomenon as an entropy driven prewetting (EDPW). The dashed light curve in Fig. 8 is the prewetting line for  $R \rightarrow \infty$ , which coincides with the TPS bulk coexistence curve (solid light line) for  $X_A < X_A^w \approx 0.065$ . The converging point separates the regimes of wetting ( $X_A \geq X_A^w$ ) and nonwetting ( $X_A < X_A^w$ ).

The limiting PI transition curve for  $R \rightarrow \infty$  coincides with the bulk TPS coexistence curve, which is reached about  $R = 20$ . As  $R$  decreases the PI transition occurs at lower  $\rho_T$  values. *Hence, for a given cylinder size immersed in the bulk, we first see the PI transition, then the EDPW transition, and finally the TPS transition, as  $\rho_T$  increases.* Whether a PI or EDPW transition occur, the AB-pairs adsorption inside the pore or at the outside cylinder's surface implies that the number of AB-pairs decreases in the bulk, thereby increasing the total accessible volume. For a constant  $\rho_T$ , a larger accessible volume implies more entropy. Therefore, the cylinder's cavity and its outside surface act as an entropy reservoir.

As  $R$  decreases the prewetting line shifts towards the TPS coexistence curve, meanwhile its corresponding  $X_A^w$  is displaced towards higher values of  $X_A$  (not shown). For small values of  $R$ , the prewetting lines are in general above their corresponding PI transition curves (see Fig. 8), except for large values of  $R$  ( $R > 20$ ), where it is below its PI transition. This behavior, which at first might sound contradictory, can be understood if one realizes that the smaller the cylinder the larger the confinement inside the pore, but the smaller the confinement exerted by its outside surface, and that confinement promotes the PI or EDPW transitions.

From the perspective of the pore cavity, given that the chemical potential is the same outside and inside the cylinder, to have the same energy necessary to bring a particle A from infinity to inside or outside the pore, the inside average concentration must be smaller than that

outside, to compensate for their confinement. This effect is clearly seen in Fig. 2, in the  $\bar{\rho}_T$  curve as a function of  $\rho_T$ , and is magnified at the PI transition, i.e., the number of A-B pairs increases inside the pore after the PI transition, thereby exhibiting the transition mechanism. Since the confinement is lower at the outside pore surface the EDPW transition occurs at higher  $\rho_T$ .

Trough PI and EDPW transitions, the system adopts configurations in which the number of AB pairs are decreased as a mechanism to maximize accessible volume, i.e., entropy. That is, on one hand, the asymmetric pairs (AB) occupy a higher volume than symmetric pairs (AA or BB) and, on the other hand, particles next to a surface (inside or outside the cylinder) have a lower coordination number, both mechanisms implying an increase of accessible volume. Hence, the system uses the cylindrical cavity and its outside surface as an entropy reservoir.

#### IV. CONCLUSIONS

We have studied the adsorption of a non-additive hard sphere mixture on the inner and outer surfaces of a cylindrical nanopore. Upon approaching towards the bulk two-phase separation (but well inside the homogeneous phase) it was found a phase transition of the confined fluid, referred to as population inversion. Such a transition is identified by a sudden change in composition of the confined fluid, involving an absorption (desorption) of the less (more) concentrated species in bulk. Further increments of the bulk total number density give raise to a transition at the cylinder's outside surface, which is characterized by a preferable adsorption of the less concentrated species in bulk over the more concentrated one, referred to as entropy driven prewetting. All these phenomena, confinement induced population inversion and wetting-like transition are akin to the capillary condensation-evaporation and wetting for simple fluids. However two differences should be pointed out: 1) These novel effects occur near the fluid-fluid two phase separation, whereas for simple fluids the related phenomena occur near the gas-liquid phase transition, and 2) These effects are ruled by entropy only. The smaller cylinder the higher the confinement inside the cylinder, but lower the confinement due to the outside surface of the cylinder. The higher the confinement the lower the concentration at which the PI and EDPW transitions occur. Hence, a particular selection of particles and nano-cylinders sizes can be used for selective adsorption, in different applications.

- 
- <sup>1</sup> W. M. Gelbart, R. F. Bruinsma, P. A. Pincus, and V. A. Parsegian, *Physics Today* **53**, 38 (2000).
- <sup>2</sup> A. Striolo, A. A. Chialvo, P. T. Cummings, and K. E. Gubbins, *Langmuir* **19**, 8583 (2003).
- <sup>3</sup> K. Koga, H. Tanaka, and X. C. Zeng, *Nature* **408**, 564 (2000).
- <sup>4</sup> M. M. T. da Gama and R. Evans, *Mol. Phys.* **48**, 687 (1983).
- <sup>5</sup> J. O. Rädler, I. Koltover, T. Salditt, and C. R. Safinya, *Science* **275**, 810 (1997).
- <sup>6</sup> G. Odriozola, F. Jiménez-Ángeles, and M. Lozada-Cassou, *Phys. Rev. Lett.* **97**, 018102 (2006).
- <sup>7</sup> J. Yu, L. Degève, and M. Lozada-Cassou, *Phys. Rev. Lett.* **79**, 3656 (1997).
- <sup>8</sup> G. E. Aguilar-Pineda, F. Jiménez-Ángeles, J. Yu, and M. Lozada-Cassou, *J. Phys. Chem. B* **111**, 2033 (2007).
- <sup>9</sup> P. Tarazona, *Physica Scripta* **T19**, 369 (1987).
- <sup>10</sup> R. Evans, U. M. B. Marconi, and P. Tarazona, *J. Chem. Phys.* **84**, 2376 (1986).
- <sup>11</sup> R. Evans, U. M. B. Marconi, and P. Tarazona, *J. Chem. Soc. Faraday Trans. 2* **82**, 1763 (1986).
- <sup>12</sup> B. K. Peterson and K. E. Gubbins, *Mol. Phys.* **62**, 215 (1987).
- <sup>13</sup> X. Zhao, *Phys. Rev. B* **76**, 041402 (2007).
- <sup>14</sup> B. K. Peterson, J. P. R. B. Walton, and K. E. Gubins, *J. Chem. Soc. Faraday Trans. 2* **82**, 1789 (1986).
- <sup>15</sup> F. van Swol and J. R. Henderson, *J. Chem. Soc. Faraday Trans. 2* **82**, 1685 (1986).
- <sup>16</sup> M. Dijkstra and R. van Roij, *J. Phys.: Condens. Matter* **17**, S3507 (2005).
- <sup>17</sup> M. Schmidt, A. Fortini, and M. Dijkstra, *J. Phys.: Condens. Matter* **15**, S3411 (2003).
- <sup>18</sup> R. L. C. Vink, A. DeVirgiliis, J. Horbach, and K. Binder, *Phys. Rev. E* **74**, 031601 (2006).
- <sup>19</sup> G. Pellicane, R. L. C. Vink, and H. Löwen, *J. Phys.: Condens. Matter* **20**, 115101 (2006).
- <sup>20</sup> R. Roth and M. Kroll, *J. Phys.: Condens. Matter* **18**, 6517 (2006).
- <sup>21</sup> M. Schmidt, A. Fortini, and M. Dijkstra, *J. Phys.: Condens. Matter* **16**, S4159 (2004).
- <sup>22</sup> Y. Duda, E. Vakarin, and J. Alexandre, *J. Coll. Int. Sci.* **258**, 10 (2003).
- <sup>23</sup> O. Sierra and Y. Duda, *Phys. Lett. A* **280**, 146 (2001).
- <sup>24</sup> Y. Duda, O. Pizio, and S. Sokolowski, *J. Phys. Chem. B* **108**, 19442 (2004).
- <sup>25</sup> J. G. Amar, *Mol. Phys.* **67**, 739 (1989).
- <sup>26</sup> A. Bellemans, V. Mathot, and M. Simon, *Adv. Chem. Phys.* **11**, 117 (1967).
- <sup>27</sup> D. Gazzillo, G. Pastore, and R. Frattini, *Cond. Matt.* **2**, 8463 (1990).
- <sup>28</sup> B. Widom and J. Rowlinson, *J. Chem. Phys.* **52**, 1670 (1970).
- <sup>29</sup> A. Malijevský, S. Sokolowski, and T. Zientarski, *J. Chem. Phys.* **125**, 114505 (2006).
- <sup>30</sup> Y. Duda and F. Vazquez, *Langmuir* **21**, 1096 (2005).
- <sup>31</sup> Y. Duda, R. Govea, M. Galicia, H. Beltran, and L. Zamudio-Rivera, *J. Phys. Chem. B* **109**, 22674 (2005).
- <sup>32</sup> B. Abu-Sharkh and E. Z. Hamad, *Langmuir* **20**, 254 (2004).
- <sup>33</sup> J. A. Schouten, *Phys. Rep.* **173**, 33 (1989).
- <sup>34</sup> K. Jagannathan and A. Yethiraj, *J. Chem. Phys.* **118**, 7907 (2003).
- <sup>35</sup> A. Santos, M. L. de Haro, and S. B. Yuste, *J. Chem. Phys.* **122**, 024514 (2005).
- <sup>36</sup> E. Lomba, M. Álvarez, L. L. Lee, and N. G. Almarza, *J. Chem. Phys.* **104**, 4180 (1996).
- <sup>37</sup> G. Pellicane, C. Caccamo, F. Saija, and P. V. Giaquinta, *J. Phys. Chem. B* **111**, 4503 (2007).
- <sup>38</sup> J. Alexandre, M. Lozada-Cassou, and L. Degève, *Mol. Phys.* **88**, 1317 (1996).
- <sup>39</sup> M. Lozada-Cassou, in *Fundamentals of Inhomogeneous Fluids*, edited by D. Henderson (Marcel Dekker, New York, 1992), Chap. 8.
- <sup>40</sup> D. A. McQuarrie, *Statistical Mechanics* (Harper and Row, New York, 1976).
- <sup>41</sup> A. Z. Panagiotopoulos, *Mol. Phys.* **61**, 813 (1987).
- <sup>42</sup> E. de Miguel, E. M. del Río, and M. M. T. da Gama, *J. Chem. Phys.* **103**, 6489 (1995).
- <sup>43</sup> S. Sajjadi, F. Jahanzadb, and M. Yianneskisa, *Colloids Surfaces A: Physicochem. and Eng. Aspects* **240**, 149 (2004).
- <sup>44</sup> J. Yuan, X. Liu, O. Akbulut, J. Hu, S. L. Suib, J. Kong, and F. Stellacci, *Nature Nanotechnology* **3**, 332 (2008).